Identifying incoherent mixing effects in the coherent two-dimensional photocurrent excitation spectra of semiconductors

Cite as: J. Chem. Phys. 157, 204202 (2022); https://doi.org/10.1063/5.0121635 Submitted: 18 August 2022 • Accepted: 07 November 2022 • Accepted Manuscript Online: 07 November 2022 • Published Online: 22 November 2022





🧓 llaria Bargigia, 🔟 Elizabeth Gutiérrez-Meza, 问 David A. Valverde-Chávez, et al.







ARTICLES YOU MAY BE INTERESTED IN

Stochastic exciton-scattering theory of optical line shapes: Renormalized many-body contributions

The Journal of Chemical Physics 157, 054103 (2022); https://doi.org/10.1063/5.0095575

Renormalization of excitonic properties by polar phonons

The Journal of Chemical Physics 157, 104116 (2022); https://doi.org/10.1063/5.0100738

Coupled charge and energy transfer dynamics in light harvesting complexes from a hybrid hierarchical equations of motion approach

The Journal of Chemical Physics 157, 174104 (2022); https://doi.org/10.1063/5.0117659





Identifying incoherent mixing effects in the coherent two-dimensional photocurrent excitation spectra of semiconductors

Cite as: J. Chem. Phys. 157, 204202 (2022); doi: 10.1063/5.0121635 Submitted: 18 August 2022 • Accepted: 7 November 2022 • **Published Online: 22 November 2022**







Ilaria Bargigia, 🗓 📵 Elizabeth Gutiérrez-Meza, 🕩 David A. Valverde-Chávez, 🕩 Sarah R. Marques,



Ajay Ram Srimath Kandada, Dand Carlos Silva 1,3,4,6) **AFFILIATIONS**

- ¹ School of Chemistry and Biochemistry, Georgia Institute of Technology, 901 Atlantic Drive, Atlanta, Georgia 30332, USA
- ²Department of Physics and Center for Functional Materials, Wake Forest University, 1834 Wake Forest Road, Winston-Salem, North Carolina 27109, USA
- School of Physics, Georgia Institute of Technology, 837 State Street, Atlanta, Georgia 30332, USA
- School of Materials Science and Engineering, Georgia Institute of Technology, 771 Ferst Drive NW, Atlanta, Georgia 30332, USA
- ^{a)}Current address: Center for Nano Science and Technology@PoliMi, Istituto Italiano di Tecnologia, via Pascoli 70/3, 20133 Milano, Italy.
- b) Author to whom correspondence should be addressed: carlos.silva@gatech.edu

ABSTRACT

We have previously demonstrated that in the context of two-dimensional (2D) coherent electronic spectroscopy measured by phase modulation and phase-sensitive detection, an incoherent nonlinear response due to pairs of photoexcitations produced via linear excitation pathways contributes to the measured signal as an unexpected background [Grégoire et al., J. Chem. Phys. 147, 114201 (2017)]. Here, we simulate the effect of such incoherent population mixing in the photocurrent signal collected from a GaAs solar cell by acting externally on the transimpedance amplifier circuit used for phase-sensitive detection, and we identify an effective strategy to recognize the presence of incoherent population mixing in 2D data. While we find that incoherent mixing is reflected by the crosstalk between the linear amplitudes at the two timedelay variables in the four-pulse excitation sequence, we do not observe any strict phase correlations between the coherent and incoherent contributions, as expected from modeling of a simple system.

Published under an exclusive license by AIP Publishing. https://doi.org/10.1063/5.0121635

I. INTRODUCTION

Electronic two-dimensional (2D) spectroscopy is a powerful tool to probe energetic landscapes^{1,2} as it provides relevant information about the coupling between different energy levels, their relaxation dynamics, the coupling between electronic and vibrational levels, and multi-body interactions.^{3,4} While most commonly this technique is implemented through the radiation from a non-linear time-varying coherent polarization in a phase-matched and time-ordered pulse-sequence configuration, 5-8 phase modulation and phase cycling approaches have also been developed, with the distinct advantages of allowing for a higher sensitivity and the inspection of longer population times. Furthermore, these approaches are based on the detection of action (excitation)

signals, such as photoluminescence intensity, 9-20 photocurrent, 21-24 and photoinduced absorption,²⁵ and therefore, they are suitable for measuring operating devices (e.g., solar cells and diodes).² The phase-sensitive detection scheme also offers a distinct advantage in the self-stabilization of the experiment. Nevertheless, recent studies with phase modulation and phase cycling approaches have shown that, in condensed matter systems, incoherent signals arising from nonlinear processes can distort and potentially mask the two-dimensional coherent signatures.²⁶ The sought nonlinear coherent signal originates from the interference of the quantum wave-packets generated by the four-pulse sequence. This interference produces a fourth-order excited-state population that ideally undergoes only first-order radiative and non-radiative decay processes. This signal is generally defined as "coherent" because it directly stems from the four light-matter interactions and it retains a well-defined phase pathway. In condensed-matter systems, however, there is the possibility for the excited-state population to undergo not only first-order decay processes but second-order decay processes as well (i.e., bimolecular recombination, exciton-exciton annihilation, Auger recombination, and photocarrier scattering processes). These processes result in a nonlinear signal, which is not coherent in nature, as it is the result of subsequent second-order interactions of the original excited state population produced by each pair of the four-pulse sequence. It is also important to highlight how emerging/un-optimized devices can show frequency dependent impedance and interface parasitic capacitance that make them nonlinear in nature: therefore, nonlinear signal mixing can not only be an intrinsic characteristic of the material under consideration, but it can also arise from the device architecture. As a consequence, extreme care must be taken when interpreting such 2D spectra, but this task is far from trivial. Kalaee et al. proposed a means of distinguishing the coherent from the incoherent contributions²⁷ by means of nonperturbative simulation of two-dimensional spectra in a simple two-level molecular system, assuming the presence of exciton-exciton annihilation. These authors showed that when the two excited states have different quantum yields, the incoherent contribution acquires a π phase shift relative to the coherent signal. In that scenario, it would then be enough to measure the phase of the two-dimensional coherent signal simultaneously with the phase of the linear signal to allow for the separation of incoherent multi-body dynamics and coherent excitation pathways. In our work, we build upon this input. We experimentally demonstrate how in a more complex and practical system as a bulk semiconductor the scenario is more convoluted, and separating the coherent from the incoherent component is not straightforward. In fact, contrary to what was predicted by Kalee et al. in a very simple model,²⁷ we do not observe any strict phase correlations between the coherent and incoherent contributions. However, we show that it is extremely important to acquire and carefully inspect the linear signals in the temporal domain to identify any presence of incoherent mixing by the crosstalk of these two signals. As a benchmark, we use a GaAs solar cell and modulate the amount of incoherent mixing by changing the electronic impedance of an external circuit, used to transduce and amplify the photocurrent generated in the solar cell. As we do not affect the physics of the sample itself but we act externally, the homogeneous and inhomogeneous broadening are not perturbed. At the same time, the nonlinear mixing thus produced has the same manifestations as the one generated by incoherent many-body dynamics. Herein, we provide an effective tool for recognizing this phenomenon and discuss a possible way of isolating the coherent response.

II. EXPERIMENTAL APPARATUS

For a detailed description of the phase modulation scheme adopted in the experiment, refer to Ref. 9; here, we will briefly outline its basic principle of operation. We implement a collinear four-pulse sequence to excite the semiconductor [Fig. 1(a)]. The schematic of our setup is reported in Fig. 1(b). The time interval between consecutive laser pulses ($T_{\rm rep}$) is set by the laser repetition rate, 300 kHz. Out of a single laser pulse-train, the two nested Mach–Zehnder interferometers create four replicas, as reported in

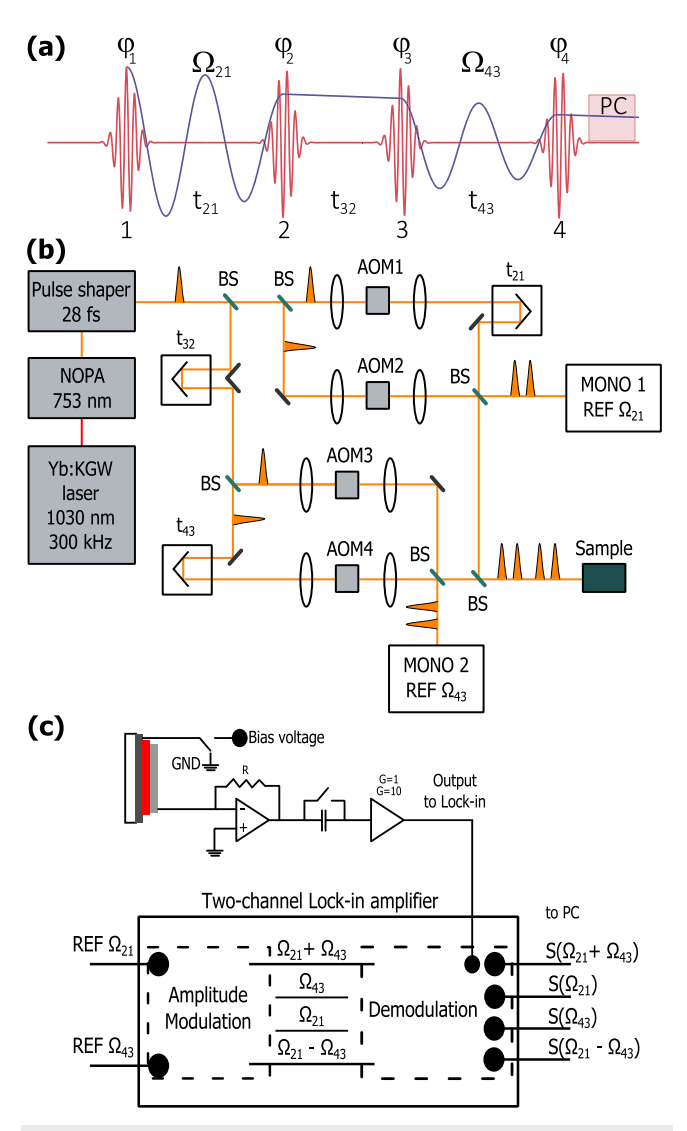


FIG. 1. (a) Schematic representation of the pulse sequence used in the experiment. Here, ϕ_i represent the phase of each pulse; t_{ji} are the inter-pulse delays and Ω_{ji} is the frequency at which the phase of each pulse oscillates. PC stands for photo-current, the integrated signal that we detect. (b) Schematic diagram of the setup for the two-dimensional spectroscopy experiment in collinear geometry. NOPA: noncollinear optical parametric amplifier. BS: beam splitter. AOM: acousto-optical modulator (Bragg cell). MONO: monochromator. REF: reference. (c) Schematic of the phase-sensitive apparatus for the photocurrent detection. The top left side represents the sample, connected to the transimpedance amplifier circuitry. The output from the TIA is fed to the digital lock-in amplifier, which is able to demodulate the signal at four different frequencies. (b) Reprinted with permission from Gutiérrez-Meza *et al.*, Sci. Adv. **7**, eabi5197 (2021) Copyright 2021. Authors licensed under a Creative Commons Attribution (CC BY) license.

Fig. 1(a). By acousto-optic modulation, each of the four replicas undergoes a frequency shift equal to the acoustic frequency Ω_i of the relative modulator. Although these frequency changes are negligible as compared to the optical frequency, they introduce a shift in the temporal phase of each pulse that oscillates at Ω_i . This means

that at each laser shot, the experiment is repeated with a sequence of pulses phase-shifted with respect to the previous shot, thus creating two collinear trains of phase-modulated pulse pairs. These two excitation pulse pairs interfere at the sample and produce a population signal oscillating at Ω_{21} and Ω_{43} in the kHz range. It can be readily shown that, within this phase cycling scheme, the non-linear signals of interest oscillate at the frequencies $\Omega_{43} - \Omega_{21}$ and $\Omega_{43} + \Omega_{21}$. In analogy to four-wave mixing experiments, $\Omega_{43} - \Omega_{21}$ and $\Omega_{43} + \Omega_{21}$ are referred to as rephasing and non-rephasing signals, respectively. These frequency components are extracted simultaneously from the overall action signal (be it a photoluminescence, a photo-induced absorption, or a photocurrent signal) by dual lock-in detection. As it is possible to see from Fig. 1(b), optical copies of pulses 1, 2 and 3, 4 are generated at the exit beam splitters of the two twin Mach-Zehnder interferometers and used to generate the reference signals for the dual lock-in demodulation. The two sets of copies are sent to two monochromators, which spectrally narrow them (thus temporally elongating them), and are then detected by using two avalanche photodiodes. The temporal elongation of the pulses provided by the monochromators produces reference signals for time delays t_{21} and t_{43} up to ~10 ps. It is important to note that, when scanning t_{21} , the phase of the references built in this way does not evolve at an optical frequency, but at a reduced frequency given by the difference between the frequency of the signal and that set by the monochromators. This frequency downshift results in an improvement of the signal-to-noise ratio inversely proportional to the frequency downshift itself, which virtually removes the impact of the mechanical fluctuations occurring in the setup on the signals of interest.9 In order to obtain the reference signals at the frequencies of the rephasing and non-rephasing signals, $\Omega_{43} - \Omega_{21}$ and $\Omega_{43} + \Omega_{21}$, one of the two photodiode outputs (typically the one at higher frequency) undergoes amplitude modulation (AM) by the output of the other photodiode. The AM signal obtained carries the two sideband frequencies of interest $(\Omega_{43} - \Omega_{21} \text{ and } \Omega_{43} + \Omega_{21})$ and can then be used for the lock-in demodulation of the action signal collected from the sample, as schematically shown in Fig. 1(c) for the specific case of a photocurrent measurement. In our case, the signal is collected from a GaAs solar cell kept under short circuit condition (i.e., zero bias) and illuminated by the sequence of the four phase-stabilized laser pulses. The photocurrent signal thus generated is converted into a voltage signal by using a transimpedance current amplifier (TIA-HF2TA Current Amplifier, Zurich Instruments) and then sent to a digital lock-in amplifier (HF2LI Zurich Instruments) for phase-sensitive detection. The 2D maps are built acquiring the demodulated signals at fixed t_{32} times and by scanning t_{21} and t_{43} ; t_{21} is called the coherence time, t_{43} is the detection time, and t_{32} is the population waiting time. Specifically, for a given

population waiting time, data are sequentially recorded at different coherence times in the interval of interest, typically extending to a few hundred femtoseconds; the detection time is then stepped, and the coherence time scanned repeatedly until the full 2D time response is recorded. Each of such scans produces eight maps, thanks to the capability of the lock-in amplifier to simultaneously demodulate the input signal at multiple frequencies: the in-phase and the in-quadrature maps for the rephasing and non-rephasing frequencies and the in-phase and in-quadrature ones for the signals oscillating at Ω_{43} and at Ω_{21} . The maps so obtained in the time domain are finally converted to the energy domain by Fourier-transforming the time variables t_{21} and t_{43} and recorded as a function of the population waiting time, t_{32} .

III. NONLINEAR INCOHERENT CONTRIBUTIONS TO THE 2D LINE SHAPE

Our strategy consists of introducing a nonlinearity in the measured signal in a controlled and simple way by acting on the TIA parameters [an electronic scheme of the circuitry can be found in Fig. 1(c)]. The total amplification of the current collected from the device, G_{TOT} , depends on the input impedance R of the first operational amplifier and on the voltage gain G of the final operational amplifier: $G_{TOT} = R \times G$. By increasing the total gain of the TIA, we can mimic not only the effect of nonlinear population mixing in the sample but also the nonlinearities arising from external factors, such as frequency dependent impedances and parasitic capacitances.

For this work, we selected three different combinations of R and G, as reported in Table I. R and G can only assume discrete values. In particular, R can be chosen as 100 V/A, 1 kV/A, 10 kV/A, 10 kV/A, 10 kV/A, 10 mV/A, or 100 mV/A. Instead, G can be either 1 or 10. The choice of R and G is mainly dictated by the maximum current that the transimpedance amplifier can accept as input, the bandwidth of the signal, and the input impedance. Given that the current coming from the solar cell at the fluence we used is $-3.4~\mu$ A and that the demodulation frequencies are in the kHz range, the values we chose are all suitable: in fact, above a G_{TOT} of 1 MV/A, the TIA is saturated as its maximum input current becomes equal or lower than $\pm 1~\mu$ A. The three combinations of R and G chosen here are those that show the lowest nonlinearity, a medium nonlinearity, and a maximum nonlinearity while keeping a good signal-to-noise ratio and avoiding saturating the TIA.

In particular, by changing the total gain, we introduce extra Fourier components in the frequency spectrum of the raw (undemodulated) output signal of the transimpedance amplifier (the voltage signal generated at the output of the TIA as it is read by

TABLE I. The three gains used.

	R (kV/A)	G	G _{TOT} (kV/A)	Bandwidth 3 dB cut-off (MHz)	Max input current range	Input impedance (Ω)
$G_{TOT,1}$	1	1	1	50	±1 mA	50
$G_{TOT,2}$	100	1	100	1.5	$\pm 10 \ \mu A$	100
$G_{TOT,3}$	10	10	100	8	±10 μA	50

the lock-in amplifier, before any demodulation, is shown in the supplementary material). These new frequency components seep in the 2D spectra. Figure 2 shows the real (left column) and imaginary (right column) components of the rephasing and the nonrephasing maps for a population waiting time of $t_{32} = 50$ fs. Maps (a), (d), (g), and (j) were collected with $G_{TOT,1}$; maps (b), (e), (h), and (k) were collected with $G_{TOT,2}$; and maps (c), (f), (i), and (l) were collected with $G_{TOT,3}$. Rephasing and nonrephasing maps taken with the lowest total gain $G_{TOT,1}$, maps (a), (d)/(g), (j), show a primarily absorptive line shape: both real and imaginary parts of the signal are dominated by a strong resonant feature lying on the diagonal and roughly centered on the laser central energy $\omega_L = 1.65$ eV. When the input impedance of the TIA circuit is increased and the total gain is $G_{TOT,2}$, slight changes appear in the rephasing and nonrephasing maps as the spectral features lose resolution. The nonrephasing signal seems to be more strongly affected: while the main positive feature in the real part of the signal remains substantially unaffected, the relative weight of the negative peaks is now more strongly favoring the lower energy feature. The maximum nonlinearity is seen for maps (c), (f)/(i), (l), recorded for $G_{TOT,3}$. Here, the nonlinear signal induces a plethora of new features, both positive and negative and both on and off the diagonal. While, if taken singularly, it is difficult to recognize the presence of incoherent mixing in these sets of maps, the time-domain maps of the **linear signals** oscillating at Ω_{21} and at Ω_{43} provide a clear indication of this phenomenon, as detailed in Sec. III A.

A. Analysis of the linear time-domain measurement

Careful inspection of the time-domain linear signals demodulated at Ω_{43} and Ω_{21} shows a dependence of the signal distribution on the total gain of the TIA, as exemplified in Fig. 3 for the normalized amplitude (left column) and phase (right column) of the signal demodulated at Ω_{43} . Let us first examine the data for the lowest gain, Figs. 3(a) and 3(d). Because we are demodulating at Ω_{43} , the amplitude is expected to oscillate along the t_{43} axis (for a fixed value of t_{21}) and remain constant along the t_{21} axis (for a fixed value of t_{43}). On the other hand, because our reference frequency is far from the transition resonance we are scanning, the phase shows a staircase-like behavior along t_{43} whose periodicity is related to the total bandwidth of the response. This staircase behavior has been already observed in a model quantum system, atomic 87 Rb vapor,

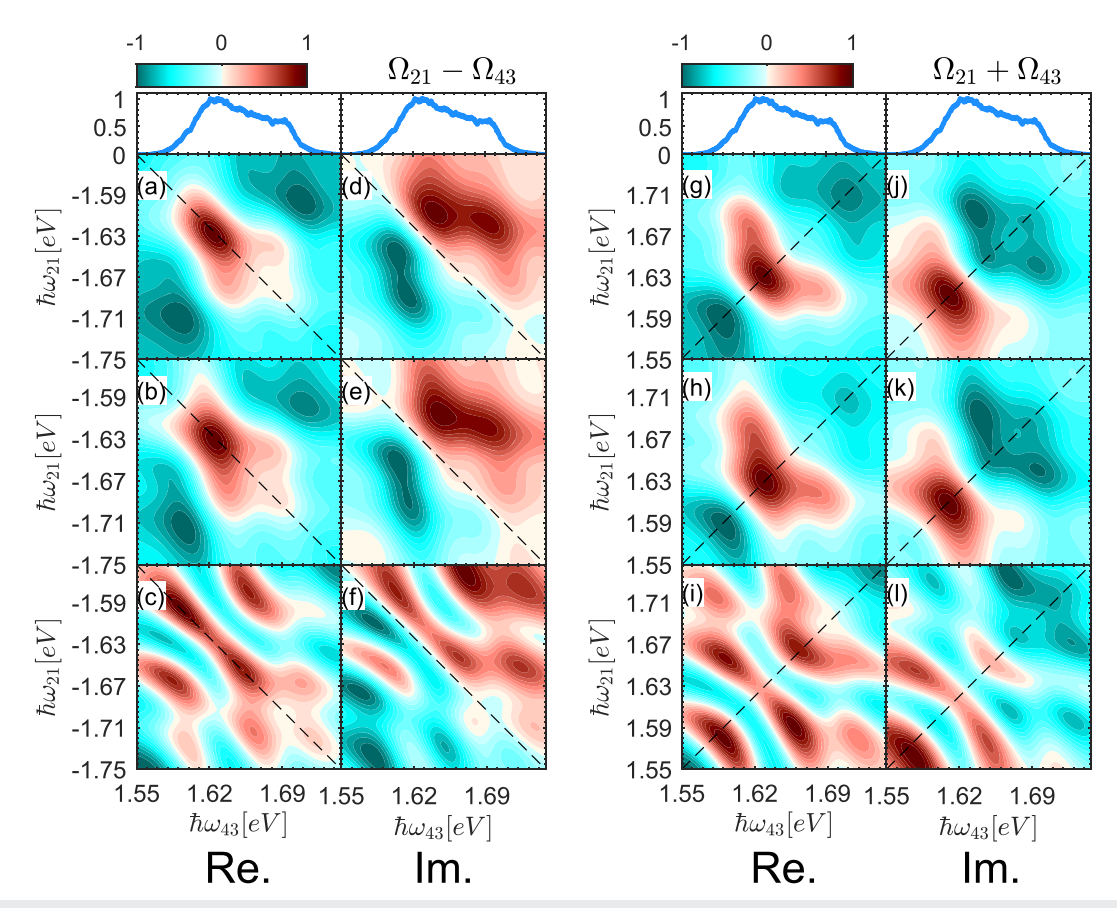


FIG. 2. Two-dimensional photo-current spectra at a population waiting time of 50 fs for the three total gains. Left: real and imaginary components of the rephasing signals for $G_{TOT,1}$ [(a) and (d)], $G_{TOT,2}$ [(b) and (e)], and $G_{TOT,3}$ [(c) and (f)]. Right: real and imaginary parts of the non-rephasing signals for $G_{TOT,1}$ [(g) and (j)], $G_{TOT,2}$ [(h) and (k)], and $G_{TOT,3}$ [(i) and (l)].

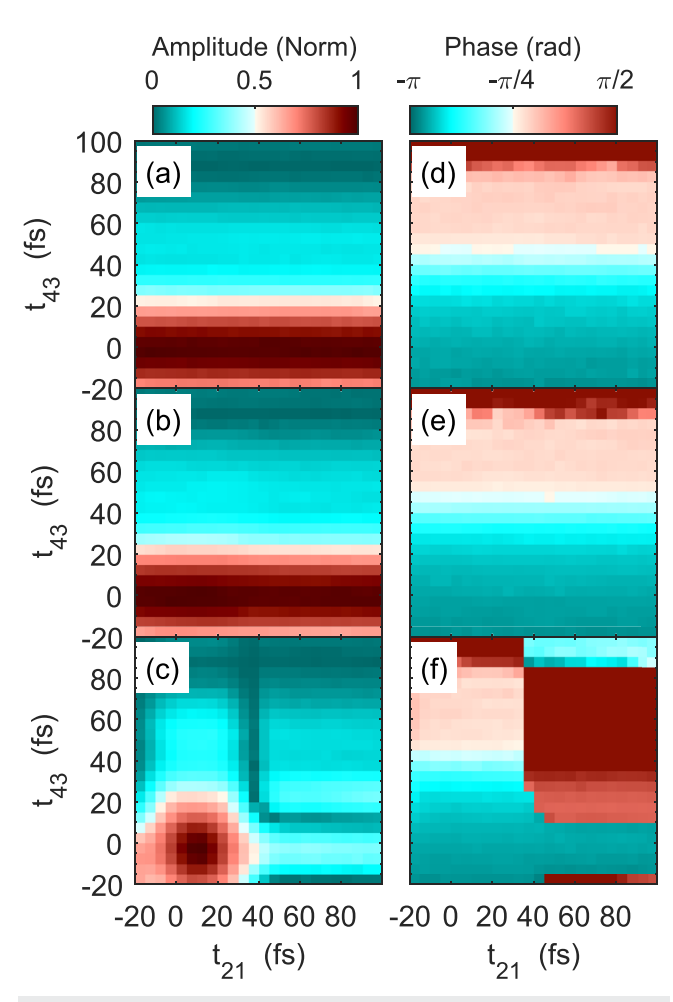


FIG. 3. Two-dimensional photo-current data in the time-domain, demodulated at Ω_{43} . (a)–(c) Amplitude of the linear signal demodulated at Ω_{43} for $G_{TOT,1}$, $G_{TOT,2}$, and $G_{TOT,3}$, respectively. (d)–(f) Phase of the linear signal demodulated at Ω_{43} for $G_{TOT,1}$, $G_{TOT,2}$, and $G_{TOT,3}$, respectively.

when the laser pulse was tuned such that the two excited state amplitudes of the D transition, $|a_1|$ and $|a_2|$, were excited with increasingly equal weight.²⁸ As expected, the phase assumes a constant value along t_{21} . By changing G_{TOT} , we introduce a non-linear component: the maps acquired for $G_{TOT,3}$ show the highest degree of nonlinearity both in the amplitude and in the phase. This behavior is more evident if we take cuts along the two orthogonal axis $t_{21} = 0$ fs and $t_{43} = 0$ fs of both amplitude and phase, Fig. 4. To better compare the amplitude cuts along the two orthogonal directions and highlight the shape of the curves, data have been normalized at 1. For $G_{TOT,1}$, we indeed see that the amplitude of the signal oscillates only along the $t_{21} = 0$ fs direction (orange dashed line), while it remains constant for the cut along $t_{43} = 0$ fs (blue solid line). As G_{TOT} is varied, the amplitude of the signal starts oscillating along $t_{43} = 0$ fs as well, with a certain time delay as it is especially evident for $G_{TOT,3}$ [Fig. 4(c)]. This is indicative of the crosstalk between the two linear channels due to nonlinear signal contributions in the amplification circuit. In this extreme case, the phase also seems to be affected, albeit in a lower measure. Comparing the last two rows, which represent data acquired at the same G_{TOT} , G seems to have a greater influence on the amount of nonlinearity introduced in the system compared with R.

These data can be interpreted in light of the formalism developed by Tekavec et al. where a two-pulse sequence originating from a single Mach-Zehnder interferometer was interacting in the sample.²⁸ For each value of the inter-pulse delay t_{ii} , the photocurrent signal gets demodulated by the lock-in amplifier at one of the phase modulation reference frequencies Ω_{ii} (j = 2 or 4 and i = 1 or 3 depending on which of the two internal interferometers is being measured). Then, the lock-in amplifier multiplies the alternatingcurrent (ac) response at a particular inter-pulse delay $S(t_{ji}, t')$ by a reference waveform $\mathcal{R}(t_{ji},t',\theta_{\rm ref})$ and then removes the ac components via a low-pass filter with characteristic time constant τ_{int} , which limits the integration time of the measurement. Here, the time variable t' is a discrete temporal variable accounting for the period of the many pulse-sequence repetitions over the integration window limited by τ_{int} . The constant reference phase that includes the spectral phase difference between the two pulses is θ_{ref} . We measure the in-phase (X, nominally with $\theta_{\text{ref }X} = 0^{\circ}$) and in-quadrature (Y, θ_{ref} $_Y = 90^{\circ}$) components of the time-integrated photocurrent, ²⁸

$$X(t_{ji}) = \frac{1}{\tau_{\text{int}}} \int_0^\infty dt' \, \mathcal{S}(t_{ji}, t') \mathcal{R}(t_{ji}, t', \theta_{\text{ref } X}) e^{-t'/\tau_{\text{int}}},$$

$$Y(t_{ji}) = \frac{1}{\tau_{\text{int}}} \int_0^\infty dt' \, \mathcal{S}(t_{ji}, t') \mathcal{R}(t_{ji}, t', \theta_{\text{ref } Y}) e^{-t'/\tau_{\text{int}}}$$

$$(1)$$

such that the total vectorial output of the amplifier is $Z(t_{ji}) = X(t_{ji}) + iY(t_{ji})$. The reference waveform is the interference contribution to the pulse-pair power spectrum,²⁸

$$\mathcal{R}(t_{ii}, t') \propto \cos[\omega_{\text{ref}}t_{ii} - \Omega_{ii}t' - \theta_{\text{ref}} + \theta_0],$$
 (2)

where $\omega_{\rm ref}$ is the central frequency determined by the monochromator MONO 1(2) in Fig. 1(a) and θ_0 is an arbitrary phase offset imposed by the lock-in amplifier. In the absence of an incoherent nonlinearity in the material response and sole contribution from the linear population $n^{(2)}$ that is due to the two-pulse sequence, the purely coherent response in a 3D semiconductor $\mathcal{S}_{\rm coh}$ is given by²⁶

$$S_{\text{coh}}(t_{ji}) \propto f(t_{ji}) \otimes n^{(2)}(t_{ji}),$$

$$n^{(2)} = \frac{2}{\hbar^2} \Re \int_{\mathbb{R}} |\mu_{eg}|^2 2\pi \left(\frac{2m^*}{\hbar^2}\right)^{3/2} \sqrt{\hbar\omega - E_g}$$

$$\times \alpha_i(\omega) \alpha_j(\omega) e^{-i\omega t_{ji} - \Gamma_{eg} t_{ji}} e^{i\phi_{ji}} d\omega,$$
(3)

where $f(t_{ji})$ is the instrument response function determined by the temporal pulse width, which must be convoluted with $n^{(2)}$. In Eq. (3), μ_{eg} is the ground-to-excited-state transition dipole moment and is multiplied by the joint density of states for a 3D semiconductor with energy gap E_g , $\alpha_{i(j)}$ is the spectral amplitude of the ith (jth) pulse, Γ_{eg} is the dephasing rate of the transition, and ϕ_{ji} is the instantaneous phase difference between the two excitation pulses, which is modulated at frequency Ω_{ji} . For spectrally identical, transform limited pulses and assuming the reference phase from the lock-in to be zero, the instantaneous phase difference is simply $\phi_{ij} = \Omega_{ji}t' + (\theta_2(\omega))$

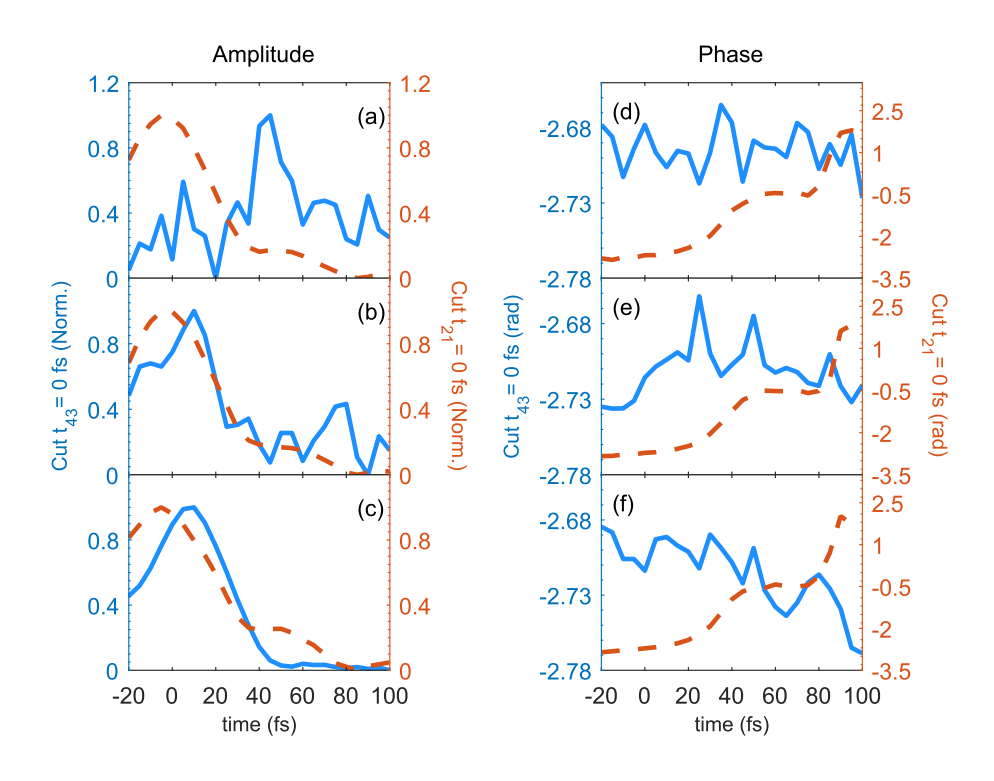


FIG. 4. (a)–(c) Cuts of the amplitude maps along the t_{43} temporal scan direction ($t_{43}=0$ fs, blue, left axis) and the t_{21} direction ($t_{21}=0$ fs, red, right axis) for $G_{TOT,1}$, $G_{TOT,2}$, and $G_{TOT,3}$, respectively, for the signal demodulated at Ω_{43} . (d)–(f) Cuts of the phase maps along the t_{43} temporal scan direction ($t_{43}=0$ fs, blue, left axis) and the t_{21} direction ($t_{21}=0$ fs, red, right axis) for $G_{TOT,2}$, and $G_{TOT,3}$, respectively, for the signal demodulated at Ω_{43} .

 $-\theta_1(\omega)$) + $\theta_0 = \Omega_{ji}t'$, Ω_{ji} being the difference in the frequencies of the two acousto-optic modulators. Inserting Eq. (3) into Eq. (1), we can find the expressions for $X(t_{ji})$ and $Y(t_{ji})$,

$$X(t_{ji}) = f(t_{ji}) \otimes \int_{\mathbb{R}} d\omega \mid \mu_{eg} \mid^{2} 2\pi \left(\frac{2m^{*}}{\hbar^{2}}\right)^{3/2} \sqrt{\hbar\omega - E_{g}}$$

$$\times \alpha_{i}(\omega)\alpha_{j}(\omega) \cos[-(\omega - \omega_{ref})t_{ji}]e^{(-\Gamma_{ji}t_{ji})},$$

$$Y(t_{ji}) = f(t_{ji}) \otimes \int_{\mathbb{R}} d\omega \mid \mu_{eg} \mid^{2} 2\pi \left(\frac{2m^{*}}{\hbar^{2}}\right)^{3/2} \sqrt{\hbar\omega - E_{g}}$$

$$\times \alpha_{i}(\omega)\alpha_{i}(\omega) \sin[-(\omega - \omega_{ref})t_{ji}]e^{(-\Gamma_{ji}t_{ji})}.$$

$$(4)$$

Using Eq. (4), we can simulate the amplitude $A(t_{ji})$ = $\sqrt{X^2(t_{ij}) + Y^2(t_{ij})}$ and the phase $\Theta(t_{ij})$ of the signal acquired in the specific case of GaAs (see the supplementary material for details) and compare them with the experimental data: results are reported in Figs. 5(a) and 5(b). We can see that there is good qualitative agreement with the data characterized by the least contribution of nonlinear mixing: the amplitude is a slowly decaying function, while the phase is a monotonically non-decreasing function. There are, however, aspects of simulations, which pertain to the modeling of the semiconductor that we are not able to properly capture, for example, our simulations show a sharp 2π jump in the phase. As it is not the scope of this paper, the modeling of a layered GaAs solar cell, we will not study this behavior in detail. We explicitly note that this formalism does not show any dependence of the signal demodulated at Ω_{43} on t_{21} : this stems from the fact that it was specifically developed without taking into account the effects of nonlinear mixing, which we are discussing here and, as in Fig. 3, do cause a crosstalk between the two temporal axes.

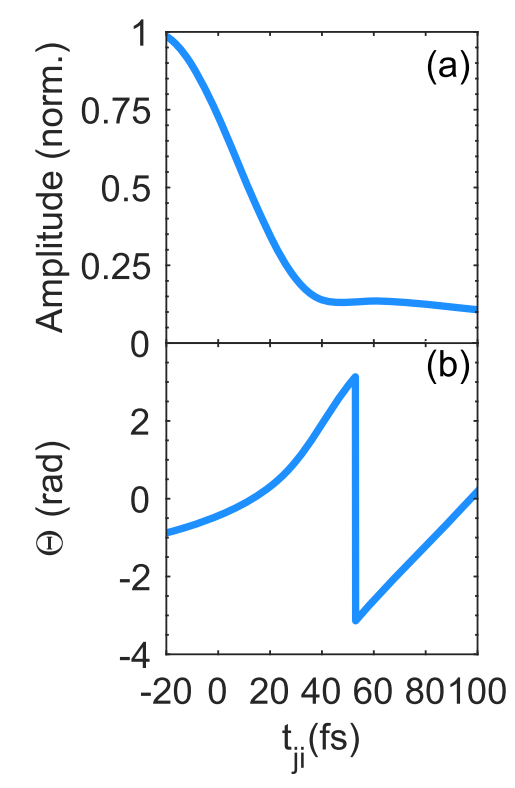


FIG. 5. (a) Simulated amplitude of the total signal $Z(t_{ji}) = X(t_{ji}) + iY(t_{ji})$, obtained using Eq. (4) for a two-pulse experiment. (b) Simulated phase of $Z(t_{ji}) = X(t_{ji}) + iY(t_{ji})$, obtained using Eq. (4) for a two-pulse experiment.

B. Analysis of the time-domain four-pulse measurement

The time-domain phase and amplitude maps corresponding to the 2D spectra for the nonrephasing signal are reported in Fig. 6 (see the supplementary material for the rephasing maps). In both cases, the gain has a strong impact on the amplitude spectrum, whereas the phase is mostly unaffected by the nonlinearity introduced in the system. The different noise level observed between the different maps is to be expected as the gain of the conversion from the photocurrent to voltage signal is progressively changed. While the time-domain maps of the linear signals oscillating at Ω_{21} and at Ω_{43} clearly show signs of nonlinear mixing, it is more difficult to discern any hint of this phenomenon in the time-domain data for the nonrephasing and rephasing signals. We can write the total coherent response $\mathcal{S}_{\mathrm{coh}}$ as

$$S_{\text{coh}} \propto f(t_{ji}) \otimes \left[n^{(2)}(t_{ji}) + n^{(2)}(t_{lk}) + n^{(4)}(t_{ji}, t_{lk}; t_{kj}) \right],$$
 (5)

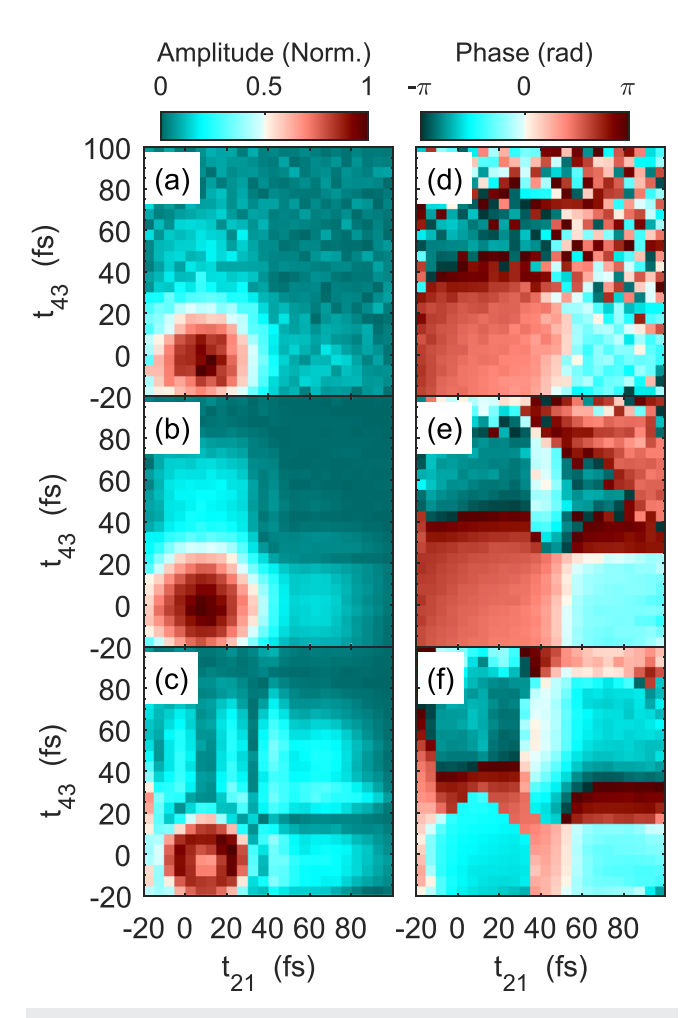


FIG. 6. (a)–(c) Amplitude of the nonrephasing signal demodulated at $\Omega_{43} + \Omega_{21}$ for $G_{707,1}$, $G_{707,2}$, and $G_{707,3}$, respectively. (d)–(f) Phase of the nonrephasing signal demodulated at $\Omega_{43} + \Omega_{21}$ for $G_{707,1}$, $G_{707,2}$, and $G_{707,3}$, respectively.

where $n^{(4)}(t_{ji}, t_{lk}; t_{kj})$ is the fourth order population responsible for the coherent response of the material,

$$n^{(4)}(t_{ij}, t_{kl}; t_{kj}) = S_4(t_{43}, t_{21}) + S_1(t_{43}, t_{21}, t_{32}) + S_3(t_{43}, t_{21}) + S_2(t_{43}, t_{21}, t_{32}) = \langle \psi_4 | \psi_{321} \rangle + \langle \psi_{432} | \psi_1 \rangle + \langle \psi_{421} | \psi_3 \rangle + \langle \psi_{431} | \psi_2 \rangle.$$
 (6)

 $S_4(t_{43},t_{21})$ and $S_1(t_{43},t_{21},t_{32})$ are the nonrephasing components, whereas $S_3(t_{43},t_{21})$ and $S_2(t_{43},t_{21},t_{32})$ are the rephasing parts of the signal. Our detected signal is the result of the superposition of the coherent response of the GaAs solar cell $\mathcal{S}_{\rm coh}$ and a nonlinear contribution. In a 3D semiconductor as GaAs, it is not that trivial to isolate these two components.

IV. DISCUSSION

Incoherent population mixing can heavily impair the correct interpretation of 2D spectra of condensed-matter systems. It is therefore important to recognize when these effects are predominant and when we can instead neglect them. We recently discussed the presence of Frenkel biexcitons in a model of a hybrid HJ photophysical aggregate polymer using 2D photoluminescence excitation spectroscopy.¹⁸ In that context, the analysis of the amplitude temporal spectra showed no crosstalk between the two time axes, thus ruling out incoherent mixing effects. The reason behind this is that the fluence was low enough not to generate substantial interparticle interactions. As a general rule of thumb, in fact, nonlinear population dynamics become sufficiently important to mask the true coherent response of the material the more the photoexcitations are mobile and subjected to reciprocal interactions (e.g., scattering processes, Auger recombination, and bimolecular annihilation processes). While the effort of discerning the coherent signal from the incoherent one based on the assumption that they show a definite phase difference has shown some potential in theoretical simulations of a specific two-level molecular system,²⁷ this approach may not be applicable, in general. In this work, we introduce different degrees of nonlinearity by changing the electronic impedance of the external transduction circuitry. By using the formalism developed by Tekavec et al.,28 we are able to appropriately simulate the coherent photocurrent signal originating from a two-pulse experiment: discrepancies between our simulations and the data can be attributed to our assumption of a parabolic density of states, where in actuality the system has a non-parabolic dispersion. When we introduce higher nonlinearities in the system, however, there is no apparent simple link between the phases of the coherent and incoherent contributions. The results obtained by Kalaee et al.²⁷ are based on the assumption of a simplistic three-level system where the only means of recombination is exciton-exciton annihilation. In real-world, complicated systems, the complexity of the interactions requires a different approach to the problem. Inspired by the work developed by Grégoire et al.,26 where they assumed a weak bimolecular annihilation and the time-integrated signal had a quadratic dependence from the initial population density, we expand S_{tot} as a power series, where β_i are constants,

$$S_{\text{tot}} \sim \beta_0 + \beta_1 S_{coh}^1 + \beta_2 S_{coh}^2 + \mathcal{O}(S_{coh}). \tag{7}$$

As a first approximation, we can limit the expansion at the second order. S_{coh}^2 is the time-varying function that accounts for the incoherent population contributions. We can expand S_{coh}^2 by squaring the terms that appear in Eq. (5), thus obtaining a series of terms that oscillate at various frequencies (see the supplementary material for details). Some of these oscillation frequencies correspond to the sum frequency $\Phi_{43} + \Phi_{21}$ and to Φ_{43} ,

$$2S_{21}(t_{21}, \Phi_{21}) \cdot S_{43}(t_{43}, \Phi_{43}) = 8\Re \sum_{a} \left[|\mu_{ag}|^2 \alpha^2(\omega_{ag}) \right]^2 \times e^{-i\omega_{ag}(t_{43} + t_{21})} e^{i\Phi_{SUM}},$$
(8)

$$2S_{21}(t_{21}, \Phi_{21}) \cdot S_3(t_{43}, t_{21}, \Phi_{DIFF})$$

$$= 8\Re \sum |\mu_{ag}|^4 \mu_{bg}^2 \alpha^4(\omega_{ag}) \alpha^2(\omega_{bg}) e^{-i\omega_{ag}(t_{43} + t_{21})} e^{i\omega_{bg}t_{21}} e^{i\Phi_{43}}, \quad (9)$$

$$2S_{21}(t_{21}, \Phi_{21}) \cdot S_{2}(t_{43}, t_{21}, \Phi_{DIFF})$$

$$= 8\Re \sum_{\alpha} |\mu_{ag}|^{4} \mu_{bg}^{2} \alpha^{4} (\omega_{ag}) \alpha^{2} (\omega_{bg}) e^{-i(\omega_{ag} - \omega_{bg})t_{21}}$$

$$\times e^{-i\omega_{ag}t_{43} - i(\omega_{ag} - \omega_{bg})t_{32}} e^{i\Phi_{43}}. \tag{10}$$

These terms oscillate with a component depending on $t_{43} + t_{21}$, t_{21} , t_{43} , and t_{32} , in agreement with what we experimentally see in the time domain maps of the linear and the nonrephasing nonlinear signals. We do not find any terms oscillating at the rephasing frequency or at Φ_{21} . This could explain why the nonrephasing part is more strongly affected by the nonlinearity. However, this conclusion rests on a truncated expansion: by considering higher order terms, components oscillating at a combination of the phases could become important.

Empirically, it seems that our system can be intrinsically described by an expansion in power terms. The question remains if this is a correct assumption, and if so, how we can determine the coefficients β_i in Eq. (7). These coefficients hold the key to the prospect of disentangling the coherent from the incoherent contributions. A possible way to recover these coefficients could be to develop a circuit analysis, in analogy to what is routinely done for electrochemical impedance spectroscopy, for instance. By building an equivalent circuit of the system under investigation, it could be possible to extract the information needed to reconstruct Eq. (7). An important point that needs to be addressed is the universality of Eq. (7) and, in a correlated but distinct way, of the coefficients β_i . Both the power terms in Eq. (7) and the coefficients could be directly related to the physical origin of nonlinear mixing, and in this case, they could be different depending on the specific process, for example, for an external electric response or for bimolecular recombination vs Auger recombination. An indication that there are higher order terms playing a substantial role is given by the presence of higher order harmonics in the detected photocurrent signal. We use only two phase-locked pulses and set the lock-in to pick up components oscillating at integer multiples of the reference frequency, $m\Omega_{ii}$, m = 1, 2, 3, 4. The results can be found in Fig. 7 as a function of the fluence. The signal at the fundamental frequency is linear in a log-log scale for the range of fluences tested here. At low fluence, the signal for higher order harmonics starts around two orders of magnitude below the signal at Ω_{ii} , but the gap in the amplitudes closes at higher fluences. We can also note a change in the slope of the

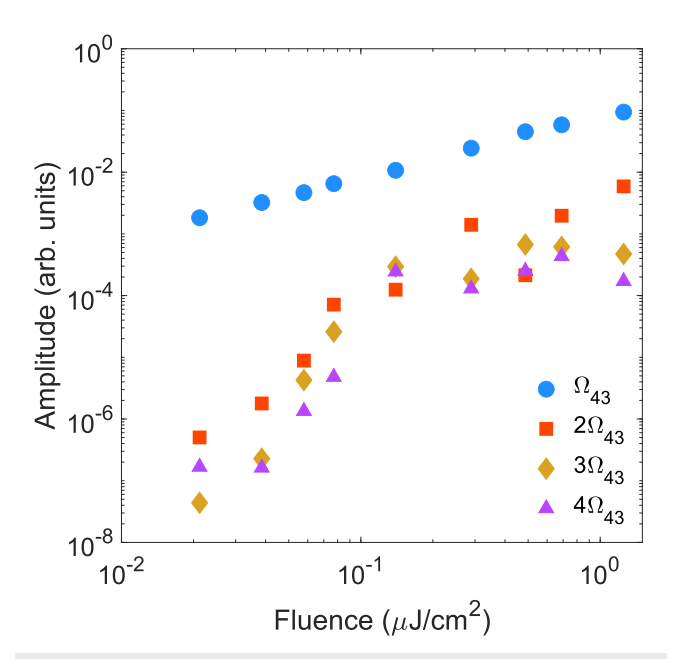


FIG. 7. Fluence dependence of the photocurrent signal collected in a two-pulse experiment and demodulated at frequencies $m\Omega_{43}$, m=1-4.

amplitudes of $m\Omega_{ji}$, where above 0.1 μ J/cm², the trend becomes sublinear. These higher order terms come either from an mth coherent excited state or from higher order terms in the expansion of Eq. (5). Although much lower than the fundamental signal, $m\Omega_{ji}$ signals are still relevant due to the extremely high signal-to-noise ratio typical of phase-sensitive techniques and can easily mask the coherent signal or cause a misinterpretation of 2D data. It is therefore important to be able to detect the presence of incoherent mixing by acquiring and carefully inspecting simultaneously both the nonlinear and linear maps in the time-domain.

V. CONCLUSIONS AND OUTLOOK

In this paper, we used the electronic impedance of an external transimpedance amplifier circuit to simulate nonlinearity in the photocurrent signal from a model GaAs solar cell. We showed that in a real-case scenario, the link between the phases of the coherent and incoherent contributions is not trivial, and we propose a way of recognizing the presence of incoherent mixing in 2D data by simultaneously acquiring the linear signals and analyzing their behavior in the time domain. Incoherent mixing will cause the linear signal to oscillate also along the temporal axis associated with the pulse-pairs whose frequency the lock-in is looking at and not only along the orthogonal one. We empirically derive a power series of the purely coherent response S_{coh} that generates terms oscillating at the nonrephasing frequency and at Φ_{43} : these terms depend on $t_{43} + t_{21}$, t_{21} , t_{43} , and t_{32} , in agreement with the experimental evidence. Further investigation is needed to validate the reasonableness and universality of our hypothesis and to unravel the connection between the proposed power series and the physical processes, leading to nonlinear mixing. A possible way would be to develop an equivalent circuit modeling the system under study, which could phenomenologically

take into account all the phenomena involved in the incoherent mixing.

SUPPLEMENTARY MATERIAL

See the supplementary material for the details of the setup and of the GaAs solar cell; the maps in the time domain of the rephasing signal and details on the simulation of the two pulse experiment for a GaAs solar cell; and, finally, the calculations of S_{co}^2 .

ACKNOWLEDGMENTS

The authors are grateful to Professor Ned Ekins-Daukes for providing the GaAs solar cells needed for the study. C.S. acknowledges the support from the National Science Foundation (Grant No. DMR-1904293) and from the School of Chemistry and Biochemistry and the College of Science of Georgia Institute of Technology.

AUTHOR DECLARATIONS

Conflict of Interest

The authors have no conflicts to disclose.

Author Contributions

Ilaria Bargigia: Formal analysis (lead); Investigation (lead); Supervision (supporting); Writing - original draft (lead); Writing - review & editing (equal). Elizabeth Gutiérrez-Meza: Formal analysis (supporting); Investigation (supporting); Writing - review & editing (supporting). David A. Valverde-Chávez: Investigation (supporting); Methodology (supporting); Writing - review & editing (supporting). Sarah R. Marques: Formal analysis (supporting); Investigation (supporting). Ajay Ram SrimathKandada: Supervision (equal); Writing - original draft (supporting); Writing - review & editing (supporting). Carlos Silva: Conceptualization (lead); Funding acquisition (lead); Project administration (lead); Supervision (lead); Visualization (equal); Writing – original draft (supporting); Writing – review & editing (lead).

DATA AVAILABILITY

The data that support the findings of this study are available from the corresponding author upon reasonable request.

REFERENCES

- ¹D. Abramavicius, D. V. Voronine, and S. Mukamel, "Unravelling coherent dynamics and energy dissipation in photosynthetic complexes by 2D spectroscopy," Biophys. J. 94, 3613-3619 (2008).
- ²S. Biswas, J. W. Kim, X. Zhang, and G. D. Scholes, "Coherent two-dimensional and broadband electronic spectroscopies," Chem. Rev. 122, 4257-4321 (2022).
- ³M. Cho, "Coherent two-dimensional optical spectroscopy," Chem. Rev. 108, 1331-1418 (2008).
- ⁴Y. Song, S. N. Clafton, R. D. Pensack, T. W. Kee, and G. D. Scholes, "Vibrational coherence probes the mechanism of ultrafast electron transfer in polymer-fullerene blends," Nat. Commun. 5, 4933 (2014).

- ⁵D. Brida, C. Manzoni, and G. Cerullo, "Phase-locked pulses for two-dimensional spectroscopy by a birefringent delay line," Opt. Lett. 37, 3027-3029 (2012).
- ⁶B. Lomsadze and S. T. Cundiff, "Frequency combs enable rapid and highresolution multidimensional coherent spectroscopy," Science 357, 1389-1391
- ⁷D. B. Turner, P. Wen, D. H. Arias, and K. A. Nelson, "Coherent two-exciton dynamics measured using two-quantum rephasing two-dimensional electronic spectroscopy," Phys. Rev. B 84, 165321 (2011).
- ⁸M. Schröter, T. Pullerits, and O. Kühn, "Using fluorescence detected twodimensional spectroscopy to investigate initial exciton delocalization between coupled chromophores," J. Chem. Phys. 149, 114107 (2018).
- ⁹P. F. Tekavec, G. A. Lott, and A. H. Marcus, "Fluorescence-detected two-dimensional electronic coherence spectroscopy by acousto-optic phase modulation," J. Chem. Phys. 127, 214307 (2007).
- ¹⁰F. D. Fuller and J. P. Ogilvie, "Experimental implementations of twodimensional fourier transform electronic spectroscopy," Annu. Rev. Phys. Chem.
- ¹¹K. J. Karki and M. F. Ciappina, "Advances in nonlinear spectroscopy using phase modulated light fields: Prospective applications in perturbative and non-perturbative regimes," Adv. Phys. X 7, 2090856 (2022).
- 12G. A. Lott, A. Perdomo-Ortiz, J. K. Utterback, J. R. Widom, A. Aspuru-Guzik, and A. H. Marcus, "Conformation of self-assembled porphyrin dimers in liposome vesicles by phase-modulation 2D fluorescence spectroscopy," Proc. Natl. Acad. Sci. U. S. A. 108, 16521-16526 (2011).
- 13 A. Perdomo-Ortiz, J. R. Widom, G. A. Lott, A. Aspuru-Guzik, and A. H. Marcus, "Conformation and electronic population transfer in membrane-supported selfassembled porphyrin dimers by 2D fluorescence spectroscopy," J. Phys. Chem. B 116, 10757-10770 (2012).
- ¹⁴J. R. Widom, N. P. Johnson, P. H. von Hippel, and A. H. Marcus, "Solution conformation of 2-aminopurine dinucleotide determined by ultraviolet twodimensional fluorescence spectroscopy," New J. Phys. 15, 025028 (2013).
- ¹⁵P. Grégoire, E. Vella, M. Dyson, C. M. Bazán, R. Leonelli, N. Stingelin, P. N. Stavrinou, E. R. Bittner, and C. Silva, "Excitonic coupling dominates the homogeneous photoluminescence excitation linewidth in semicrystalline polymeric semiconductors," Phys. Rev. B, 95 180201 (2017).
- 16P. Malý and T. Mančal, "Signatures of exciton delocalization and excitonexciton annihilation in fluorescence-detected two-dimensional coherent spectroscopy," J. Phys. Chem. Lett. 9, 5654-5659 (2018).
- ¹⁷D. Heussman, J. Kittell, L. Kringle, A. Tamimi, P. H. von Hippel, and A. H. Marcus, "Measuring local conformations and conformational disorder of (Cy3)2 dimer labeled DNA fork junctions using absorbance, circular dichroism and twodimensional fluorescence spectroscopy," Faraday Discuss. 216, 211-235 (2019).
- ¹⁸E. Gutiérrez-Meza, R. Malatesta, H. Li, I. Bargigia, A. R. S. Kandada, D. A. Valverde-Chávez, S.-M. Kim, H. Li, N. Stingelin, S. Tretiak, E. R. Bittner, and C. Silva-Acuña, "Frenkel biexcitons in hybrid HJ photophysical aggregates," Sci. Adv. 7, eabi5197 (2021).
- ¹⁹D. Agathangelou, A. Javed, F. Sessa, X. Solinas, M. Joffre, and J. P. Ogilvie, "Phase-modulated rapid-scanning fluorescence-detected two-dimensional electronic spectroscopy," J. Chem. Phys. 155, 094201 (2021).
- ²⁰D. Heussman, J. Kittell, P. H. von Hippel, and A. H. Marcus, "Temperaturedependent local conformations and conformational distributions of cyanine dimer labeled single-stranded-double-stranded DNA junctions by 2D fluorescence spectroscopy," J. Chem. Phys. 156, 045101 (2022).
- $^{\mathbf{21}}$ G. Nardin, T. M. Autry, K. L. Silverman, and S. T. Cundiff, "Multidimensional coherent photocurrent spectroscopy of a semiconductor nanostructure," Opt. Express 21, 28617 (2013).
- ²²K. J. Karki, J. R. Widom, J. Seibt, I. Moody, M. C. Lonergan, T. Pullerits, and A. H. Marcus, "Coherent two-dimensional photocurrent spectroscopy in a PbS quantum dot photocell," Nat. Commun. 5, 5869 (2014).
- A. A. Bakulin, C. Silva, and E. Vella, "Ultrafast spectroscopy with photocurrent detection: Watching excitonic optoelectronic systems at work," J. Phys. Chem. Lett. 7, 250-258 (2016).

- ²⁴E. Vella, H. Li, P. Grégoire, S. M. Tuladhar, M. S. Vezie, S. Few, C. M. Bazán, J. Nelson, C. Silva-Acuña, and E. R. Bittner, "Ultrafast decoherence dynamics govern photocarrier generation efficiencies in polymer solar cells," Sci. Rep. 6, 29437 (2016).
- ²⁵H. Li, A. Gauthier-Houle, P. Grégoire, E. Vella, C. Silva-Acuña, and E. R. Bittner, "Probing polaron excitation spectra in organic semiconductors by photoinduced-absorption-detected two-dimensional coherent spectroscopy," Chem. Phys. **481**, 281–286 (2016).
- ²⁶P. Grégoire, A. R. Srimath Kandada, E. Vella, C. Tao, R. Leonelli, and C. Silva, "Incoherent population mixing contributions to phase-modulation two-dimensional coherent excitation spectra," J. Chem. Phys. 147, 114201 (2017).
 ²⁷A. A. S. Kalaee, F. Damtie, and K. J. Karki, "Differentiation of true nonlinear and incoherent mixing of linear signals in action-detected 2D spectroscopy," J. Phys. Chem. A 123, 4119–4124 (2019).
- ²⁸ P. F. Tekavec, T. R. Dyke, and A. H. Marcus, "Wave packet interferometry and quantum state reconstruction by acousto-optic phase modulation," J. Chem. Phys. **125**, 194303 (2006).